Article

Automatic Localization Algorithm for Ultrasound Breast Tumors Based on Human Visual Mechanism

Yuting Xie [1], Ke Chen [2] and Jiangli Lin [2,*]

[1] Department of Biomedical Engineering, Sichuan University, No.24 Yihuan Road, Chengdu, China; yting_xie@hotmail.com

[2] Department of Biomedical Engineering, Sichuan University, No.24 Yihuan Road, Chengdu, China; chenke@scu.edu.cn

* Correspondence: linjiangli@scu.edu.cn; Tel.: +86-139-8191-1859

Abstract: Human visual system (HVM) can quickly localize the most salient object in scenes, which has been widely applied on natural image recognition [15]-[19]. In ultrasound (US) breast images, compared with surrounding areas, tumor is more salient because of its higher contrast. In this paper, we develop a novel automatic localization method based on HVM for automatic segmentation of US breast tumors. First intensity, blackness ratio, and superpixel contrast features are combined to compute saliency map, in which Winner Take All algorithm is used to localize the most salient region, presenting with a circle on the localized target. Finally the circle is taken as the initial contour of CV level set to finish the extraction of breast tumor. Combined with the proposed method, CV level set can achieve the fully automatic segmentation of US breast tumors. By combing intensity, blackness ratio and superpixel contrast features, the proposed localization method can successfully avoid the interference caused by background areas with low echo and high intensity. The localization method has been tested on 400 US beast images, among which 378 images succeed in localization, with high accuracy 92.00%.

Keywords: automatic localization; human visual mechanism; superpixel contrast feature; ultrasound breast tumor.

1. Introduction

Breast cancer is one of the most common malignant tumors in women, whose incidence and mortality both account the first place in women's disease and even hold a rising trend. Early diagnosis is the most effective means of prevention of breast cancer. Recent studies show that computer-aided diagnosis software based on artificial intelligence provides the possibility of early diagnosis, in which the automatic segmentation of tumors become the critical step and bottleneck.

Ultrasound, CT and MRI are clinically used for lesion imaging, among which ultrasound imaging has been widely used by doctors to diagnose breast tumors due to its non-invasion and non-ionization radiation and non-injury[1]. On the other hand, the shortcomings of ultrasound imaging, like low contrast and serious speckle noise, make it difficult to segment lesions in Ultrasound images. While level set can be used to address this challenge[2], which is currently one of the most effective segmentation methods of ultrasound images [3-7]. For level set segmentation algorithms, automatic positioning is the most critical link and also most difficult part. In fact, automatic initializing contour

is still not well solved. Although manual marking the lesion areas can be used as an alternative method, subjective deviation can greatly reduce segmentation efficiency, and artificial intervention also makes it impossible to realize the fully automatic software.

At present, automatic localization methods can be divided into two classes: point-based methods [8-9] and region-based methods [10-12].

Madabhushi et.al [9] proposed an automatic seeds point localization method. They used the accurate boundaries labeled by physicians to calculate the gray level distribution and texture distribution of tumors, and then found a reference point based on experience. In their method, pixels closer to the reference point have greater possibility to be in tumor region. This method is sensitive to speckle noise because of its pixel-based classification. Besides, the reference point assumption is unreasonable, and also influenced by physicians' operation habits.

Some researchers have proposed region-based detection methods [10-12]. Yap [11] et. al presented a region-based automatic tumor localization method, which mainly considers two factors to select object region, the size and the distance of each region to the reference point. Compared to Madabhushi's method, this method has better performance in case of noise immunity, while in some US images, if the tumors are small and there are large areas of artifacts, the right ROI is unable to be selected by this method.

Liu [12] presented a ROI automatically generation method based on SVM classifier. He divided the images into 16×16 blocks, and calculated the Gray Level Co-occurrence Matrix(GLCM) of each region as the training data of his SVM classifier. While this localization method needs many post-processing operations to select ROI, including removing linear connected areas, filling holes and experience-based region selection. Only depending on the local texture feature, this method can not separate tumor areas from normal tissues. In addition, this method is unable to localize tumors in small size and also large tumors shown in section 5.

In this paper, we propose a novel automatic localization method of US breast images. Our attention system is based on Itti HVM model [13], and according to the characteristics of US images, we use the intensity feature and blackness ratio feature to compute the saliency map. In addition, in order to avoid the drawbacks of point-based methods, we add the region-based superpixel contrast feature [14] to compute the saliency map. Unlike the other region-based methods, we did not divide input images into blocks of same size, instead simply, but also divided input images into superpixels. In each superpixel, the gray values of pixels are approximative. These three features greatly improve the performance of this model, especially the localization of tumors with large size and also some pretty small tumors.

This paper is organized as follows. Proposed object-localization algorithm is explained in Section 2. CV level set is illustrated in Section 3. The experimental results are presented in Section 4. Section 5 is the discussion on experimental results. In Section 6 conclusions and future work are presented.

2. Localization Based on HVM

Human eye, working as a biological photoelectric sensor, can quickly get visual information. This information can stimulate the visual light sensitive cells, producing electrical pulses, and guiding the eye movement. Different visual information causes different stimulation on the visual light sensitive cells, and the most significant information can get the attention of the human eyes. Human visual mechanism has been successfully applied in the field of image processing [15]-[19],

which can quickly localize the part of interest, and automatically discard the unimportant part, saving a lot of image post-processing time.

In HVM, the movement of human eyes is mainly determined by visual features. So in HVM models, feature extraction is the most important part. At present, there are many features applied in HVM models, for example, color, intensity and orientation features in Itti model. However, color and orientation features are invalid to localize tumors in US images. In our model, we use intensity, blackness ratio and superpixel contrast features to achieve tumor detection.

2.1 features

2.1.1. intensity

In US breast images, the intensity of tumor regions are different from that of its surrounding areas. So in is obviously that in respect to intensity feature, the tumor is salient because of its great contrast, and that intensity is a valid feature for tumor detection. Intensity map M_I is defined as:

$$M_I = (r + g + b)/3 \tag{1}$$

Where r, g and b are respectively the red, green and blue color components of the input image.

2.1.2. blackness ratio

In general, tumor usually presents in dark area, blackness ratio is also an effective feature to describe tumors.

Black ratio map M_{BR} is explained as:

$$M_{BR} = \frac{1 - \min(r, g, b)}{(r + g + b)/3 + \varepsilon} \tag{2}$$

To avoid influence at localization with (r+g+b)=0, ⊚ is added in function (2), where ⊚ is set to 0.001.

2.1.3. superpixel saliency

To reduce the influence of speckle noise and the post-processing complexity, input image is divided into superpixel image, in which adjacent pixels with similar texture, color and intensity are classified as a pixel block. We use simple linear iterative clustering (SLIC) [14] to yield superpixel image. Compared to existing superpixel methods, SLIC has been shown to outperform in respect to algorithm speed, memory efficiency, boundary adherence. Besides, SLIC algorithm can segment the gray images with excellent performance, shown in Figure 1b.

Preprints (www.preprints.org) | NOT PEER-REVIEWED | Posted: 5 April 2017 doi:10.20944/preprints201704.0030.v1

Peer-reviewed version available at Sensors 2017, 17, , 1101; doi:10.3390/s17051101

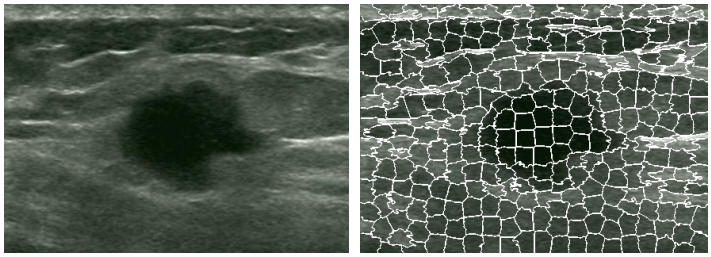

(a) Original image (b) Superpixel image

Figure 1. SLIC used to divide original image.

Superpixel saliency map is computed as:

$$S_{SP}(r_k) = W(r_k) \sum_{i=1, i\neq k}^{K} \left\{ \frac{n_i}{N} e^{-\frac{d^2(r_k, r_i)}{2\delta^2}} D(r_k, r_i) \right\}, \ \mathrm{k} = 1,2,\ldots,\mathrm{K} \tag{3}$$

$$W(r_k) = \frac{\max(\mathbf{g}) - g_k}{(\max(\mathbf{g}) - \min(\mathbf{g}))}, \ \mathbf{g} = \{g_1, g_2, \ldots, g_K\} \tag{4}$$

$$\mathrm{d}(r_k, r_i) = \sqrt{(x_k - x_i)^2 + (y_k - y_i)^2} \tag{5}$$

$$D(r_k, r_i) = g_k - g_i \tag{6}$$

In function (3), K is the number of superpixels, N and n_i are respectively the total number of pixels in input image and in superpixel r_i, δ is used to control the influence of surrounding superpixels on superpixel being computed. In function (4) and (5), $\mathbf{g}$ is the set of average gray values g_k of all superpixels. (x_k, y_k) and (x_i, y_i) in function (6) are the centroids of r_k and r_i, $d(r_k, r_i)$ is then normalized to a range of [0,1].

Based on the above function, in our method, three factors are considered: (a) Compared with normal tissues, tumor is lower echo area, making it more salient than other areas. This is achieved by weight $W(r_k)$. (b) For a superpixel, the distances to other superpixels affect the contrast values, closer superpixels have greater influence on its contrast, as illustrated by parameter $e^{-\frac{d^2(r_k, r_i)}{2\delta^2}}$ in function (3), in which δ controls the influence of surrounding superpixels r_i on current superpixel r_k in respect to euclidean distance. In our method, δ is set to 0.05 to reduce the contribution of far superpixels. (c) Larger areas denote greater effect on other areas, illustrated with parameter $\frac{n_i}{N}$.

2.2 HVM model

Preprints (www.preprints.org) | NOT PEER-REVIEWED | Posted: 5 April 2017 doi:10.20944/preprints201704.0030.v1

Peer-reviewed version available at Sensors 2017, 17, , 1101; doi:10.3390/s17051101

This localization method can be divided into four steps: (a) getting feature maps and contrast maps of blackness ratio and intensity features, (b) computing the superpixel saliency map of input image, (c) combining all saliency maps to compute the saliency map, and (d) locating the most salient region. The framework of the automated object localization method is shown in Fig2.

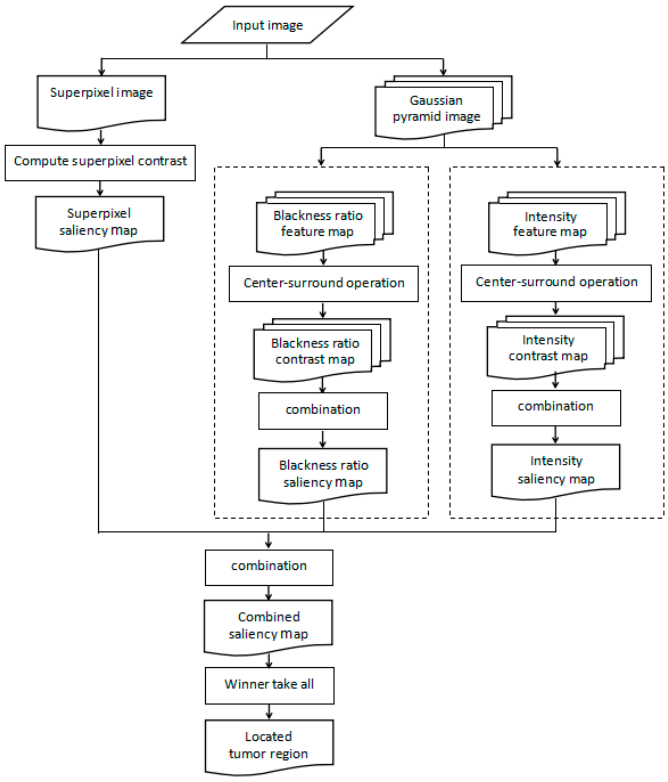

Figure 2. Proposed methodology

In this algorithm, to avoid information loss through subsampling process, firstly the input image is smoothed by convolution with a linearly separable Gaussian filter and then subsampled by a factor of two [19]. In our model, we use a 6×6 linearly separable Gaussian kernel filter [1, 5, 10, 10, 5, 1, 1]/32. The next levels $\sigma = [1,2,\ldots,9]$ of the pyramid are obtained by repeating the subsampling and decimation processes. $\sigma = 1$ represents the input image I. The resolution of layer σ is the 1/2σtimes of the original image, this representation can effectively reduce time complexity of the algorithm. The Gaussian pyramid of input image is shown in Figure 3. We can see from Figure 3 that images in higher levels have lower resolution, and that the information in object area is well retained, improving the efficiency of the procedure.

Preprints (www.preprints.org) | NOT PEER-REVIEWED | Posted: 5 April 2017 doi:10.20944/preprints201704.0030.v1

Peer-reviewed version available at Sensors 2017, 17, , 1101; doi:10.3390/s17051101

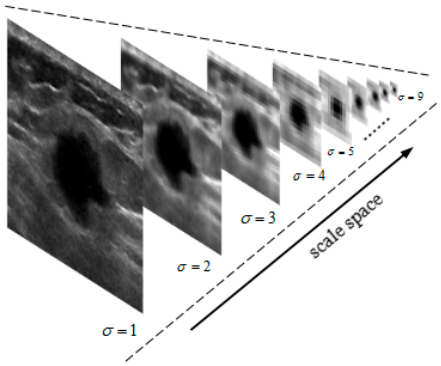

Figure 3. Gaussian pyramid of input image

2.2.1. intensity and black ratio saliency maps

Obtain the intensity and blackness ratio maps of each image pyramid and repeat for pyramid level $\sigma = [1,2,...,9]$ to get the intensity pyramid $M_I(\sigma)$ and blackness ratio pyramid $M_{BR}(\sigma)$.

Center-surround receptive fields are simulated by across-scale subtraction between two maps at the center (c) and the surround (s) levels in these pyramids, yielding contrast maps.

$$\begin{aligned} C_I(c,s) &= N\{|\, M_I(c) \Theta M_I(s) \,|\} \\ C_{BR}(c,s) &= N\{|\, M_{BR}(c) \Theta M_{BR}(s) \,|\} \end{aligned} \tag{7}$$

Where $N\{.\}$ is an iterative, nonlinear normalization operator, simulating local competition between neighboring salient localization. For the simulations in this paper, between one and five iterations are used. The contrast maps are summed over by across-scale addition $\oplus$ to the $\sigma = 5$ level. Then the sums are normalized again, generating saliency map, as shown in Figure 4.

$$\begin{aligned} S_I &= N\left(\bigoplus_{c=3}^{5}\bigoplus_{s=c+3}^{c+4} C_I\right) \\ S_{BR} &= N\left(\bigoplus_{c=3}^{5}\bigoplus_{s=c+3}^{c+4} C_{BR}\right) \end{aligned} \tag{8}$$

Figure 4a is the intensity saliency map of input image, in which some high-intensity areas have the higher conspicuity than tumor area, and other black background areas are less salient with salient value near to zero. In blackness ratio saliency map shown in Figure 4b, tumor area has the highest saliency than any other regions. Besides, some low intensity background areas are also salient.

Peer-reviewed version available at Sensors 2017, 17, , 1101; doi:10.3390/s17051101

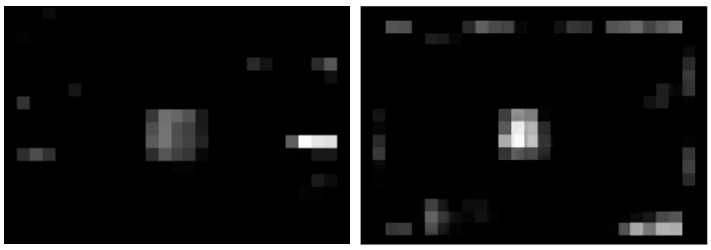

(a) Intensity saliency map (b) Blackness ratio saliency map

Figure 4. Saliency maps of intensity and blackness ratio features

2.2.2. superpixel contrast map

Firstly, the input image is divided into superpixels, which, in US images, can help reduce the influence of the speckle noise and also greatly decrease the computation complexity. In this model, we use Simple Linear Iterative Clustering (SLIC) [14] to generate superpixels. Combined with original image in Figure 5a, it is clear that in superpixel saliency map in Figure 5b, superpixels in tumor area all have relatively high conspicuity, and that in other areas, for example the high-intensity areas in the left parts of input image, are less salient because of their small areas and also pretty smaller number of same gray values as illustrated in function(3).

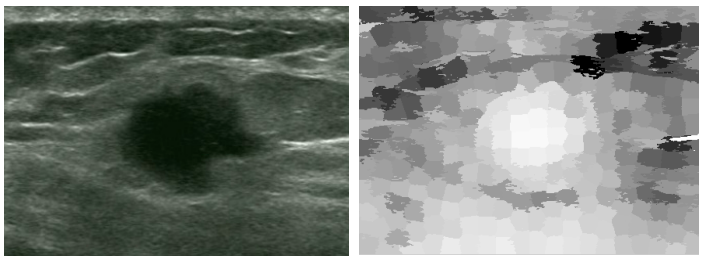

(a) Original image (b) Superpixel saliency map

Figure 5. Original image and superpixel saliency map.

2.2.3. total saliency map

$$S = \sum_{l \in \{I, BR, SP\}} S_l \tag{9}$$

We have analyzed above that the conspicuity of tumor area is greatly affected by high-intensity background areas and low-intensity background areas, respectively in intensity saliency map and black ratio saliency map. In addition, illustrated in Section 2.2, in superpixel saliency map, spindly

Peer-reviewed version available at Sensors 2017, 17, , 1101; doi:10.3390/s17051101

high-intensity areas are far less salient due to their smaller sizes. Therefore, by combining these three saliency maps, we can effectively reduce the salient values of dark background areas and also high-intensity background areas, as shown in combined saliency map in Figure 6.

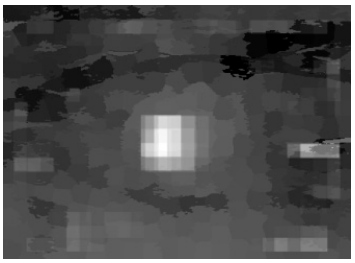

Figure 6. Combined saliency map

2.2.4. Winner Take All

Winner-take-all (WTA) neural networks have been extensively discussed as a way of making decisions. The maximum of the saliency map defines the most salient image localization, to which the focus of attention (FOA) should be directed, as shown in Figure 7. For our model, we use the WTA network proposed by Itti et al. [19-20], in which saliency map is modeled as a 2D layer of leaky integrate-and-fire neurons. These model neurons consist of a capacitance which integrates the charge delivered by synaptic input, of a leakage conductance, and of a voltage threshold.

The saliency map neurons receive excitatory from the values of saliency map x_i . The potential of saliency map neurons at more salient localization hence increases faster, and each neuron excites its corresponding WTA neuron independently, until the most salient saliency map neuron first reaches threshold and fires.

$$y_i = \begin{cases} 0 & if\ x_i < \max(X) \\ 255 & if\ x_i = \max(X) \end{cases} \qquad (10)$$
$$X = \{x_1, x_2, \ldots, x_N\}$$

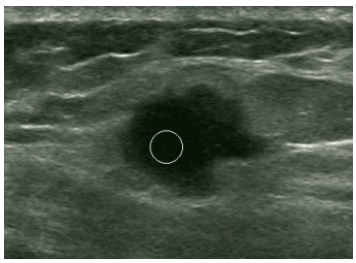

Figure 7. Localized tumor region.

3. CV Level Set

CV level set model evolves curve by minimizing the energy function instead of gradient information, it has a certain ability of noise resistance. Therefore it performs well in ultrasonic images [21]. CV level set model hypothesizes that an image consists of two piecewise smooth areas: target Ω_t and background Ω_b. The object energy function is defined as:

$$E^{CV}(C, c_t, c_b) = \lambda \iint_{\Omega t} (I - c_t)^2 dxdy + \lambda \iint_{\Omega b} (I - c_b)^2 dxdy + L(C) \tag{11}$$

where λ is the weighting coefficient, $L(C)$ is the length of the closed contour curve C. c_t and c_b are respectively the average gray value of target area and background area.

In function (11), $\lambda \iint_{\Omega t} (I - c_t)^2 dxdy$ and $\lambda \iint_{\Omega b} (I - c_b)^2 dxdy$ are fidelity terms, when the edge of the closed contour curve C coincidences with the target boundary, the sum of this two items receives a minimum value. Therefore, when the energy function obtains the minimum value, the corresponding C is the ideal contour [21].

In order to get the minimum value of energy function, plug $C(t) = \{(x, y) | \phi(t, x, y) = 0\}$ into (11)

$$E^{CV}(\phi, ct, cb) = \lambda \iint_{\Omega} [H_\varepsilon(\phi)(I - c_t)^2 + (1 - H_\varepsilon(\phi))(I - c_b)^2] dxdy + \iint_{\Omega} \delta_\varepsilon(\phi) |\nabla \phi| dxdy \tag{12}$$

Minimize the energy function to get the numerical solution of level set function:

$$\frac{\partial \phi}{\partial t} = \delta_\varepsilon(\phi) \{\nabla \cdot \frac{\nabla \phi}{|\nabla \phi|} - \lambda[(I - c_t)^2 - (I - c_b)^2]\} \tag{13}$$

The approximate regularization:

$$H_\varepsilon(\phi) = \frac{1}{2}(1 + \frac{2}{\pi} \arctan(\frac{\phi}{\varepsilon})) \tag{14}$$

$$\delta_\varepsilon(\phi) = \frac{1}{\pi} \cdot \frac{\varepsilon}{\phi^2 + \varepsilon^2} \tag{15}$$

$$\phi(x) = \begin{cases} dist(x, C) & x \text{ is on the outside of } C \\ 0 & x \text{ is on the } C \\ -dist(x, C) & x \text{ is on the inside of } C \end{cases} \tag{16}$$

4. Experimentation

An algorithm for localization and segmentation of the US breast images has been tested in this section. To evaluate the proposed algorithm, 400 US breast images from ultrasound department of West China Hospital of Sichuan University are tested. After tumor localization by proposed method, images are further processed through CV level set to extract precise contour of tumor region.

Figure 8 shows the localization and segmentation results of other six US breast images. As seen in the first line, although there are a lot of low echo areas to interfere localization, the saliency map computed by the proposed human visual model has the highest contrast value in tumor region, making it successful to position the tumor by WTA operation. In the second and third lines, these two US breast images both have high intensity backgrounds, in which blackness ratio feature maps denote most to the salient values in tumor region than other two features. As illustrated in Section 2, blackness ratio feature is able to inhibit the value of high intensity regions but enhance that of the tumor area, making the attention model able to avoid the influence of high-intensity areas. In the last two lines, tumors are pretty small with complex backgrounds, proposed method can still recognize the tumors.

Preprints (www.preprints.org) | NOT PEER-REVIEWED | Posted: 5 April 2017 doi:10.20944/preprints201704.0030.v1

Peer-reviewed version available at Sensors 2017, 17, , 1101; doi:10.3390/s17051101

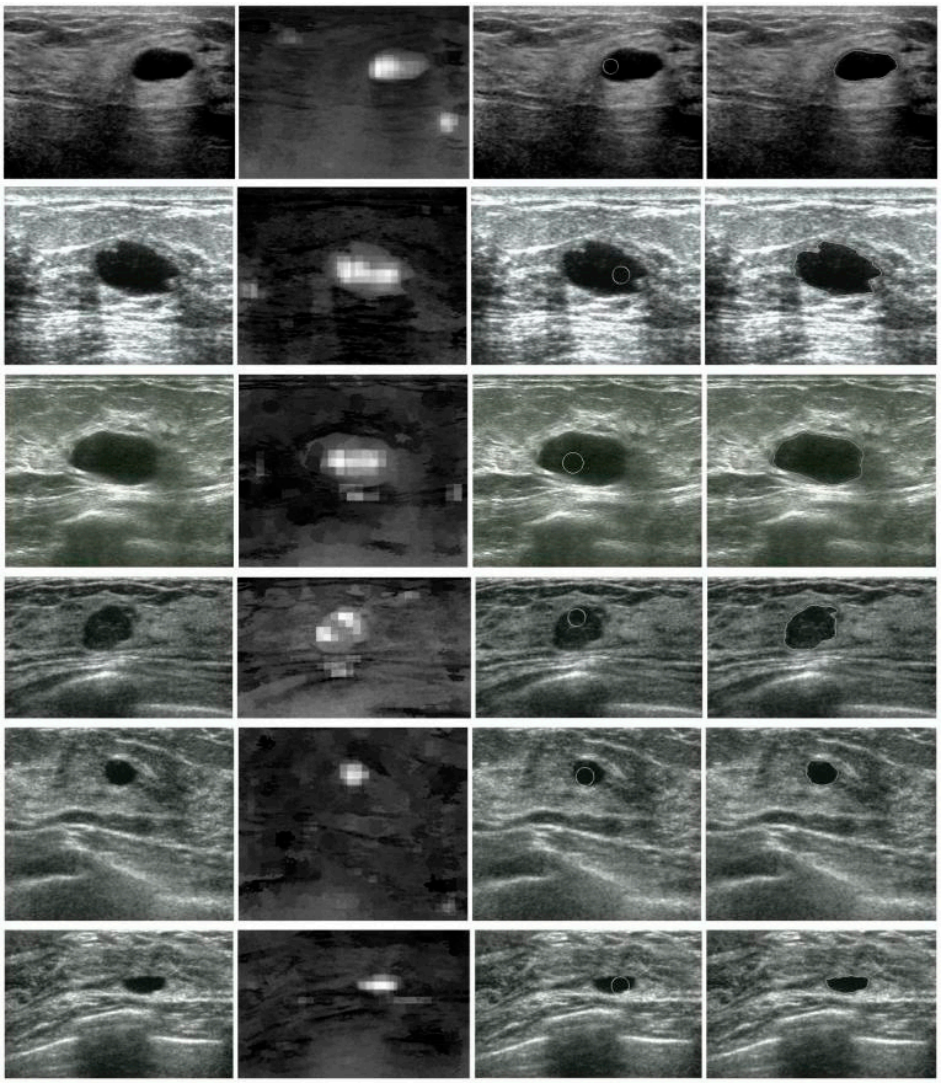

(a) original image (b) saliency map (c)localization result (d)segmentation result

Figure 8. Results of six US breast images by proposed level set method.

5. Discussion

In this section, we compare our method with the Liu's detection method[12]. The localization accuracy is illustrated in TABLE 1.

TABLE 1. The localization accuracy of Liu's method and proposed method.

Method	Liu's method	proposed method
right localization	325	368
wrong localization	75	32

Accuracy	81.25%	92.00%

TABLE 2. The right and wrong localization results of Liu's method and proposed method.

Liu's method / proposed method	**right localization**	**wrong localization**	**sum**
right localization	323	45	368
wrong localization	2	30	32
sum	325	75	400

Compared with Liu's method, the proposed method has better performance with much higher accuracy 92.00% to 81.25%, as illustrated in Table 1. The details are shown in TABLE 2. As we can see, there are 45 tumors that we have successfully positioned, while Liu's method fails. (a)-(f) show the localization results of three representative examples in this case. Figure 9a and d show big tumor covering a large area of the whole image. Liu's method is unable to detect the tumor, because in its classification process, large areas are easily mistaken as background areas. In proposed method, the saliency values of tumor area depend on the intensity and blackness ratio of tumor area[12], so the size of the tumor area does not affect our localization.

Liu's method is also unable to localize tumors in images with large areas of artifacts and also tumors with smaller size, shown respectively in Figure 9b and c, Figure 9e and f. In our model, input image is divided into superpixel image, and the saliency value of each superpixel in tumor area does not depend on the total size of tumor but the size of the superpixel itself. Besides, in intensity saliency map, saliency value of tumor area relies on the contrast to its surroundings, other than background areas. As a result, tumors can be successfully localized in those images.

Peer-reviewed version available at Sensors 2017, 17, , 1101; doi:10.3390/s17051101

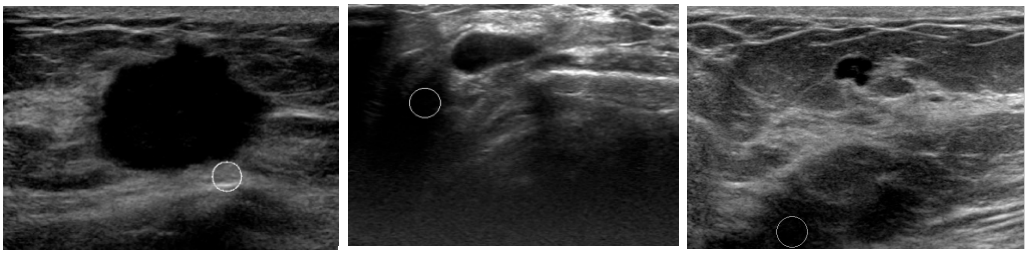

(a) Localization result by Liu's method in an image with big tumor

(b) Localization result by Liu's method in an image with large artifacts

(c) Localization result by Liu's method in an image with small tumor

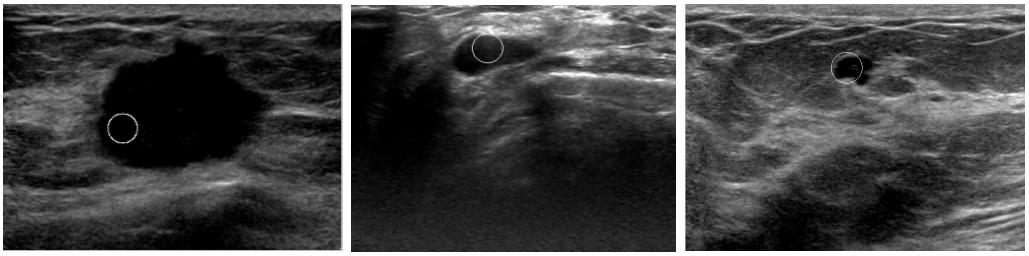

(d) Localization result by proposed method in an image with big tumor

(e) Localization result by proposed method in an image with large artifacts

(f) Localization result by proposed method in an image with small tumor

Figure 9. localization results of three images in which Liu's method failed while the proposed method succeeded.

Another case in TABLE 2 is 2 images failed in our method but localized successfully by Liu's method shown in Figure 10. In these two images, the tumor areas are of equally low intensity with some background areas as localized in Figure 10b and d, thus making the blackness ratio saliency map little contribution to tumor localization because of its equal conspicuity with those background areas. Besides, the intensity contrast of tumor areas is lower than that of those low-intensity background areas, which hold higher conspicuity than tumor areas in intensity saliency maps, as well as in superpixel saliency maps.

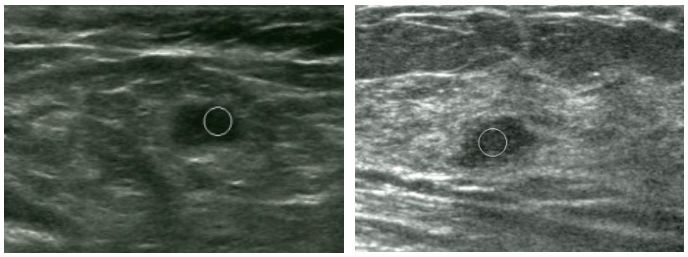

(a) Localization results by Liu's method in two images with low-contrast tumors

Peer-reviewed version available at Sensors 2017, 17, , 1101; doi:10.3390/s17051101

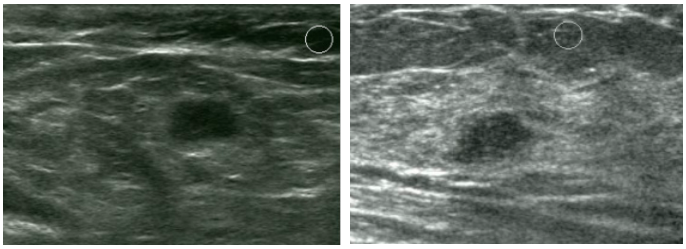

(b) Localization results by proposed method in two images with low-contrast tumors

Figure 10. Localization results of two examples in which Liu's method successfully localized tumors while the proposed method failed.

As illustrated in TABLE 2, 30 images failed by both localization methods. Figure 11 shows two examples failed by Liu's method and also proposed method. It is clear that in Figure 11a, Liu's method failed to localize tumors, because these two localized background areas are larger than tumors. In these two cases, the localized background areas have both lower echo and higher contrast than tumor areas, making the saliency value of tumors lower in blackness ratio saliency and intensity maps. Therefore, the proposed method is also unable to localize the lower saliency tumor regions.

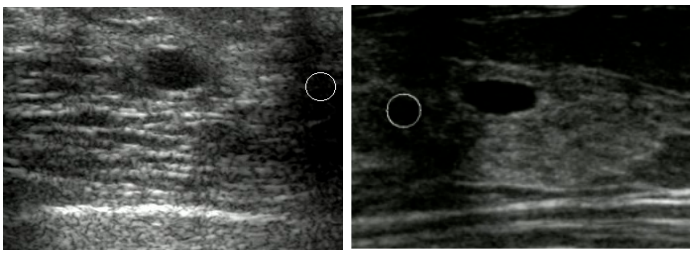

(a) Localization results by Liu's method in images where background areas have lower echo and higher contrast than tumor areas.

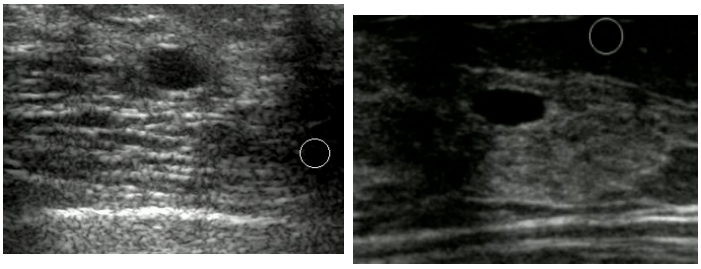

(b) Localization results by proposed method in images where background areas have lower echo and higher contrast

Figure 11. Cont. Localization results of two images in which Liu's method and proposed method both failed.

6. Concluding remarks and future work

This paper proposes a novel localization method to localize tumors in US breast images, resulting with high accuracy. In the proposed method, blackness ratio and superpixel contrast features are used to compute saliency map, with which tumors can be successfully localized without being affected by surrounding low echo and high intensity areas. Combined with this method, CV level set will no longer need the human-computer interaction to finish the extraction of tumors, achieving the fully automatic segmentation of US breast tumors.

However, this localization method also has some weakness, which is unable to localize tumors in US breast images with background areas of equally low intensity but higher contrast. In future work, according to the characteristics of tumors, we expect to improve by finding some more helpful features to structure the integrated saliency map, and also finding some methods to reduce the interference of low-intensity background areas in subcutaneous adipose layer and muscular layer, as shown in Figure 10b and Figure 11b. In addition, by combining WTA and Inhibition of Return (IOR) [13][19], multi-tumor localization would be considered in future exploration.

Acknowledgments

This paper is supported by the National Science Foundation of China Grant No.81301286, the PhD. Programs Foundation of Ministry of Education of China Grant No. 20130181120001 and Science and technology support project of Sichuan Province Grant No. 2014GZ0005. Our Images are supported by department of ultrasound, West China hospital of Sichuan university.

References

1. Liu X, Song J L, Wang S H, et al. Learning to Diagnose Cirrhosis with Liver Capsule Guided Ultrasound Image Classification. *Sensors* **2017**, 17(1):149.

2. Xiaoxia Huang B H H L. A Fast Level Set Method for Synthetic Aperture Radar Ocean Image Segmentation. *Sensors*, **2009**, 9(2):814.

3. Galluzzo F, De Marchi L, Testoni N, et al. A fully automated method for carotid plaques segmentation in ultrasound images based on motion estimation and level-set. *Ultrasonics Symposium*. *IEEE*, **2014,** 2343-2346.

4. Selvathi D, Bama S. Phase Based Distance Regularized Level Set for the segmentation of ultrasound kidney images. *Pattern Recognition Letters*, **2016**.

5. Viswanath K, Gunasundari R. Design and analysis performance of kidney stone detection from ultrasound image by level set segmentation and ANN classification. *International Conference on Advances in Computing, Communications and Informatics* **2014,** 407-414.

6. Guo, Yanhui, A. Sengur, and J. W. Tian. A novel breast ultrasound image segmentation algorithm based on neutrosophic similarity score and level set. *Computer Methods & Programs in Biomedicine* **2015**, 123, 43-53.

7. Zhou Z. Tianfu Wang, Jiangli Lin, Deyu Li, Segmentation of medical ultrasound images: novel level set approach. *Proc Spie* **2007**, 6789, 67890U-67890U-6.

8. Shan J, Cheng H D, Wang Y. A novel automatic seed point selection algorithm for breast ultrasound images. *International Conference on Pattern Recognition. IEEE*, **2008**, 1-4.

9. MADABHUSHI A, METAXAS D N. Combining low, high level and empirical domain knowledge for automated segmentation of ultrasonic breast lesions. *IEEE Trans on Medical Imaging* **2003**, 22(2), 55-169.

10. Xu Jing, Gao Xin, Fully automatic detection and segmentation algorithm for ultrasound breast images using SVM and level set. *Journal of Computer-Aided Design & Computer Graphics* **2012**, 24(5), 662-668.

11. YAP M H, EDIRISINGHE E A, FULLY H E B. Automatic lesion boundary detection in ultrasound breast images. *Proc of SPIE Medical Imaging Conference* **2007**.

12. LIU Bo, CHENG Hengda, HUANG J H, et al. Automated segmentation of ultrasonic breast lesions using statistical texture classification and active contour based on probability distance. *Ultrasound in Medicine and Biolog* **2008**, 35(8), 1309-1324.

13. Itti L, Koch C, Niebur E. A Model of Saliency-Based Visual Attention for Rapid Scene Analysis. *IEEE Transactions on Pattern Analysis & Machine Intelligence* **1998**, 20(11), 1254-1259.

14. Achanta R, Shaji A, Smith K, et al. SLIC Superpixels Compared to State-of-the-Art Superpixel Methods. *Pattern Analysis & Machine Intelligence IEEE Transactions on* **2012**, 34(11), 2274-2282.

15. Peterson H A, Rajala S A, Delp E J. Human visual system properties applied to image segmentation for image compression. *Global Telecommunications Conference* **1991,** 1, 91-95.

16. Chantelau K. Segmentation of moving images by the human visual system. *Biological Cybernetics* **1997**, 77(2), 89.

17. Jang J, Rajala S A. Segmentation based image coding using fractals and the human visual system. *International Conference on Acoustics, Speech, and Signal Processing. IEEE* **1990**, 4, 1957-1960.

18. Tsai C S, Chang C C. An improvement to image segment based on human visual system for object-based coding. *Fundamenta Informaticae* **2003**, 58(2), 167-178.

19. Walther D, Koch C. Modeling attention to salient proto-objects. *Neural Networks the Official Journal of the International Neural Network Society* **2006**, 19(9), 1395-1407.

20. Koch C, Ullman S. Shifts in selective visual attention: towards the underlying neural circuitry. *Human Neurobiology* **1985**, 4(4), 219.

21. Qian Yun, Zhang Yingjie, A survey of image segmentation methods for level set. *Journal of Image and Graphics* **2008**, 13(1), 12-18.